On the Fluid Dynamics of Shaken Bioreactors—Flow Characterization and Transition

W. Weheliye, M. Yianneskis, and A. Ducci
Dept. of Mechanical Engineering, University College London, London WC1E 7JE, U.K.

DOI 10.1002/aic.13943
Published online November 26, 2012 in Wiley Online Library (wileyonlinelibrary.com).

Phase-resolved PIV measurements were carried out to provide a thorough characterization of the flow and mixing dynamics occurring in a cylindrical shaken bioreactor when operating conditions such as medium height h, shaking rotational speed N, orbital shaking diameter d_o, and cylinder inner diameter d_i, are varied. A scaling law based on the aspect ratio h/d_i, on the orbital to cylinder diameter ratio d_o/d_i, and on the Froude number $Fr = 2(\pi N)^2 d_o/g$, is derived to predict the incipience of flow transition occurring when the free surface orientation starts to exhibit a phase delay to the shaker table position along its orbit; depending on the combination of Fr, d_o/d_i and h/d_i the transport phenomena in the bioreactor are controlled by a horizontal toroidal vortex, or by a vertical one precessing around the cylinder axis. The free surface interfacial area was directly measured by image analysis to assess oxygen transfer potential and compared to an analytical solution valid for low Fr. © 2012 American Institute of Chemical Engineers *AIChE J,* 59: 334–344, 2013
Keywords: shaken bioreactor, free surface, PIV, flow transition, mixing, transport

Introduction

In recent years microscale technology has been employed in the early stages of bioprocess development (for example, microbial fermentation, bioconversion and recovery techniques), before the developed process is implemented in a large-scale industrial stirred tank. One such microscale approach relies on the use of microwell plates, where complete mixing is achieved by shaking rather than stirring. However, despite the extended use of shaken bioreactors (flasks and microwells), it has been reported that less than 2% of the publications dealing with engineering aspects of bioreactors are dedicated to shaken bioreactors,[1] and their importance for many biochemical processes is often underestimated. To put this in perspective, a vast amount of publications on bioprocess design is already available in stirred-tank reactors (for example Escudie et al.[2]; Lavery and Nienow[3]), and accurate scaling between shaken and stirred bioreactors is hindered by the lack of engineering works for shaken devices.

Ensuring effective mixing in such devices is essential, as the presence of spatial gradients in culture parameters (e.g., dissolved gasses, concentration and shear rate) is often an important—and potentially problematic—consideration in bioreactors (Lara et al.[4]). Such gradients are often strongly affected, if not controlled, by the hydrodynamic phenomena in the bioreactors, but accurate knowledge of and information on the physical parameters affecting the cultures is lacking, while little is known about their characteristic properties, and often the few publications available provide contradictory advice concerning the most appropriate operating conditions to be employed.[1] Only relatively recently methods that facilitate the selection of optimized culture conditions have been described (Klöckner and Büchs[5]). Furthermore, larger shaken bioreactors have become available in pilot and industrial scale in the form of single-use cylindrical bags on controllable shaken platforms.[6,7] These offer a novel scale-up platform and eliminate current bottlenecks by improving process reproducibility and robustness upon scale-up. From this perspective a systematic characterization of transport phenomena in the bioreactor under different conditions is timely and necessary to derive scaling laws and parameters.

This review focuses only on fluid mechanics aspects of shaken bioreactors as they determine mixing and oxygen transfer dynamics. Few articles can be found in the literature dealing with the flow in shaken bioreactors and they have all employed computational fluid dynamics (CFD).[8,9,10] The flows in a 250-mL Erlenmeyer flask and in 24-well and 96-well bioreactors were investigated by Zhang et al.[8] and Zhang et al.[9], respectively. These studies mainly carried out a dimensional analysis to determine macroparameters such as power consumption, from the integral of the local dissipation rate, the interfacial area I_a, and the volumetric mass-transfer coefficient k_La, which are necessary to assess the overall performance of the bioreactors, but do not assess the local flow dynamics and transitions occurring at different operating conditions, and do not identify flow scaling parameters. A more detailed characterization of the flow in a cylindrical shaken bioreactor with a flat bottom is provided by the numerical simulations and experimental visualizations of Kim and Kizito,[10] who made qualitative comparisons between the space-averaged velocity flow fields obtained for various combinations of shaker rotational speed N, and fluid

Additional Supporting Information can be found in the online version of this article.

Correspondence concerning this article should be addressed to A. Ducci at a.ducci@ucl.ac.uk.

viscosity v. The numerical simulations of Discacciati et al.[11] and Zhang et al.[7] allowed visualization of the free surface shape and estimation of the interfacial area and shear stress in a cylindrical bioreactor. Experimental flow visualization in Erlenmeyer flasks carried out by Büchs et al.[12] reported first the so-called "out-of-phase" phenomenon by means of flow visualization and power consumption measurements. This phenomenon occurs at a rotational speed N, for which some of the liquid does not follow the movement of the shaking table, thus, reducing the volumetric power consumption and gas/liquid mass transfer. To distinguish between the two conditions they adapted a model of the hydrodynamics in a horizontal drum and derived a nondimensional phase number Ph (Eq. 1), which is a function of the orbital to flask diameter ratio d_o/d, and film Reynolds number Re_f, and the axial Froude number Fr_a

$$Ph = \frac{d_0}{d}(1 + 3\log_{10}(Re_f)) \tag{1}$$

In-phase conditions are obtained when $Ph > 1.26$. This model is valid only at relatively high-rotational speeds for $Fr_a > 0.4$, when the majority of the liquid is not in contact with the base of the flask.

The primary objective of this study is to address the lack of detailed knowledge of the transport/mixing processes outlined in the aforementioned review, and to enhance understanding of the phenomena involved in orbitally-shaken bioreactors. For some of the phenomena studied, techniques and methodologies previously employed to improve understanding of and optimize mixing in stirred vessels[13–17] are harnessed in this work to shed light into the corresponding processes encountered in a shaken reactor.

This study presents the first detailed description of the fluid mechanics in a cylindrical shaken bioreactor at low Froude number $Fr_a < 0.4$ in an attempt to understand both fundamental and engineering aspects of the flow, and to improve bioprocess design and scale-up by deriving a scaling law, based on physical considerations of the force dynamics in the bioreactor, that allows the prediction of the flow transition occurring at incipient out-of-phase conditions.

Materials and Methods

Phase-resolved particle image velocimetry (PIV) was used to characterize the flow in a glass cylindrical shaken bioreactor with a transparent flat bottom. A diode laser, a mirror, a Dantec intensified camera, and a cylindrical bioreactor encased in a trough were rigidly mounted on a LS—X Kühner shaker table. Schematic diagrams of the PIV system setup for measurements on vertical and horizontal planes are provided in Figure 1a and b, respectively. A magnetic encoder coupled to the shaker table and a timing box allowed synchronization of the PIV image acquisition to any orbital position of the rig. To minimize reflections at the walls and at the free surface the working fluid (water) was seeded with 50 μm rhodamine particles for the PIV measurements, while the free surface was traced with 10 μm silver coated particles. The spatial ($\Delta x_i = 1.3$ mm) and temporal ($\Delta t = 10$ ms) resolutions of the PIV measurements were optimized to fully resolve the flow macroscale features. More information on the experimental technique and algorithm developed to track the free surface can be found in Weheliye et al.[18] Experiments were carried out for two

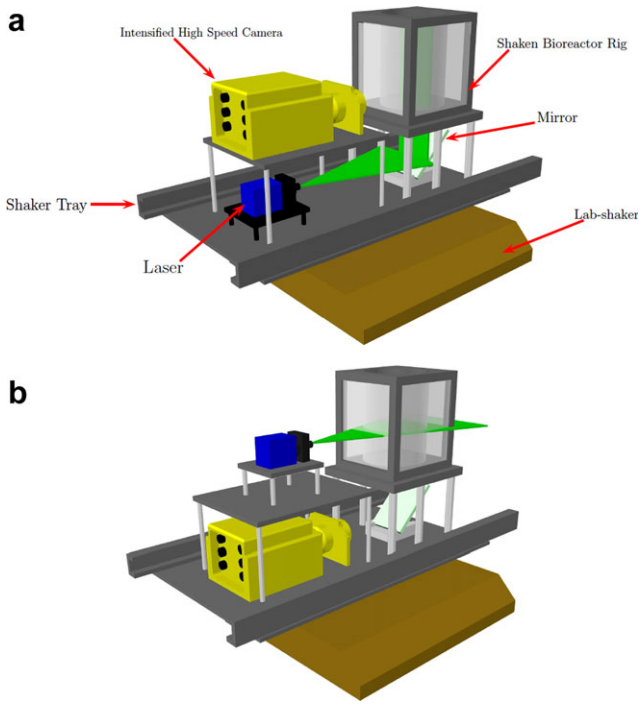

Figure 1. PIV setup configurations used to measure the velocities on (a) vertical, and (b) horizontal plane.

[Color figure can be viewed in the online issue, which is available at wileyonlinelibrary.com.]

different cylindrical bioreactors with inner diameters $d_i = 10$ cm and 13 cm for fluid heights, orbital diameters and shaker speeds in the ranges of $h = 3$–7 cm, $d_o = 1.5$–5 cm and $N = 60$–140 rpm, respectively. A cylindrical coordinate system r, φ, z is employed with the origin positioned on the cylinder axis at the bioreactor base. The origin of the angular coordinate φ identifying the position of the tray along its clockwise orbit corresponds to the point furthest to the left when the system is viewed from the top.

Results and Discussion

Characterization of in-phase flow

A description of the flow occurring in the cylindrical shaken bioreactor along its orbital motion is provided in this section. In the first part the analysis is carried out for a reference operating configuration with $h/d_i = 0.3$ and $N = 90$ rpm, while in the second part it is extended to different fluid heights, shaker speeds, orbital and cylinder diameters.

Before proceeding with the discussion it is necessary to make a short digression into the definition of the Froude number Fr, which is an essential parameter to obtain a characterization of the flow and to formulate an accurate scaling law of the bioreactor system. The Froude number is the ratio between the characteristic flow velocity and the wave propagation velocity

$$Fr = \left(\frac{v}{\sqrt{gl}}\right) \tag{2}$$

where g is the gravitational acceleration, and V and l are the flow characteristic velocity and length scale. Tissot et al.[19] used this definition, and estimated their characteristic velocity based on the average of the orbital and cylinder diameters,

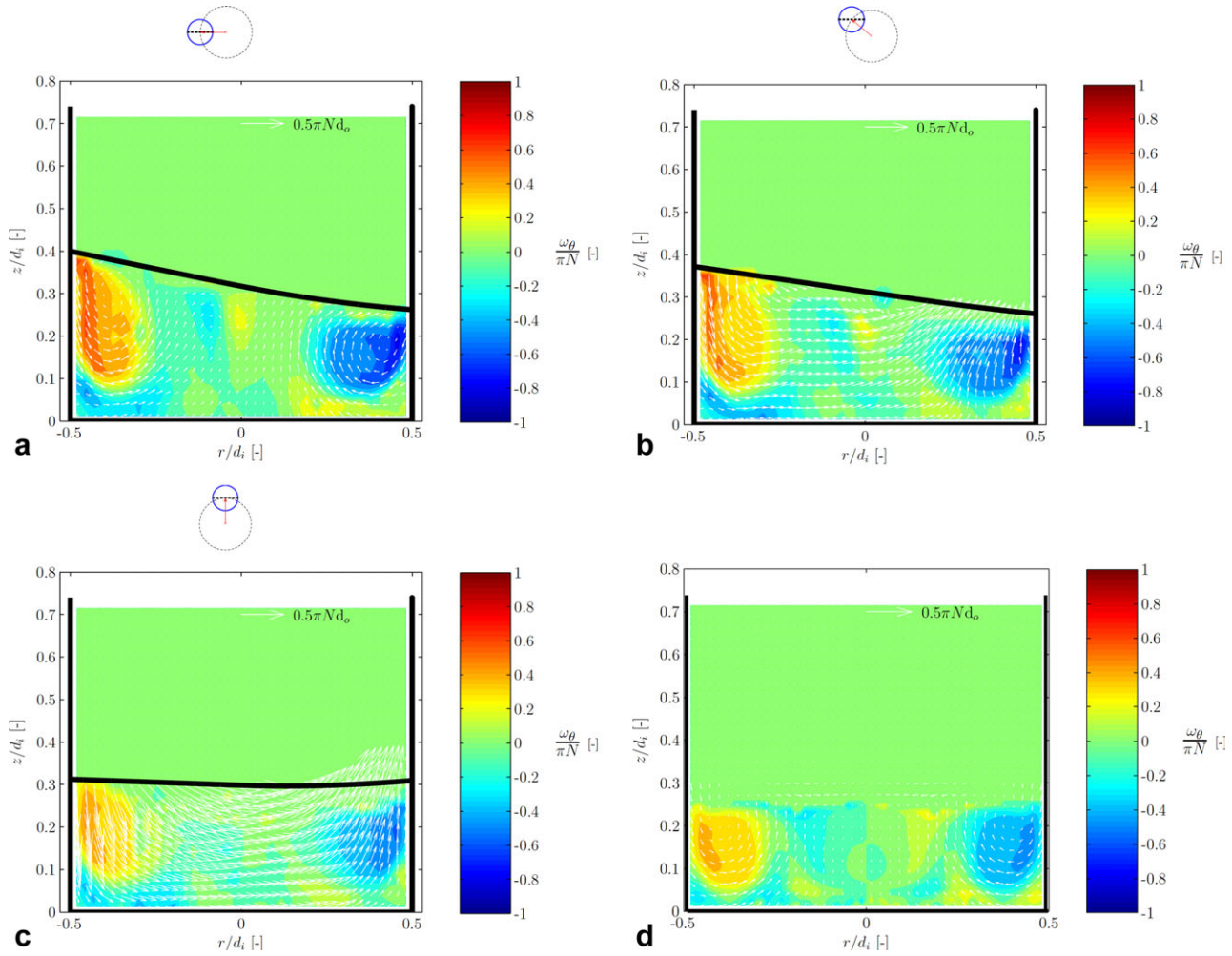

Figure 2. Phase-resolved velocity vectors and contours of the tangential component of the vorticity, ω_θ, for three different phase angles (h/d_i = 0.3, N = 90 rpm): (a) φ = 0°, (b) φ = 40°, (c) φ = 90°, and (d) ensemble-averaged velocity vectors and vorticity contours.

[Color figure can be viewed in the online issue, which is available at wileyonlinelibrary.com.]

while the inner cylinder diameter d_i, was taken as the characteristic length scale (Eq. 3)

$$Fr = \left(\frac{2\pi N(d_o + d_i)/2}{\sqrt{g d_i}}\right) \tag{3}$$

In some studies more emphasis is given to the ratio between inertial and gravitational forces, and the first power of the gravitational acceleration is employed. In these cases the definition of Fr is the squared version of that in Eq. 2.[20] In the field of shaken bioreactors, the latter definition has been extensively used by Büchs et al.[12] who distinguished between axial Fr_a and radial Fr_r Froude numbers based on Eq. 4, where the characteristic length scale used d is either the orbital or flask diameter, respectively

$$Fr = \left(\frac{2(\pi N)^2 d}{g}\right) \tag{4}$$

For consistency and in order to enable comparisons with earlier works on shaken bioreactors, the Froude number definition of Eq. 4 with the orbital diameter d_o, being the characteristic length scale is employed in this work.

The two-dimensional (2-D) phase-resolved velocity fields and contour plots of the tangential component of the vorticity ω_θ, are shown in Figure 2a–c for three phase angles, while the ensemble-averaged vector and vorticity fields are shown in Figure 2d. A sketch is provided above each plot to visualize the angular position of the cylinder (blue circle) along its orbit (dotted circle). Phase-resolved quantities were obtained by averaging 500 instantaneous velocity vector fields for each one of 18 different phase angles. Thus, the ensemble-averages were obtained over 500 × 18 = 9,000 velocity vector fields. In Figure 2a two counter-rotating vortices are observed close to the walls of the cylinder. The intensity of the two vortical structures is similar in magnitude with absolute vorticity levels varying in the range $\|\omega_\theta/(\pi N)\| = 0 - 1$. Figure 2a captures the flow field when the tray reaches its position furthest to the left, $\varphi = 0°$, and the fluid experiences the maximum centrifugal acceleration in the plane of measurement. In this case the free surface assumes its maximum inclination, and the two vortical cells are completely separated with little or no fluid being exchanged between the two.

As the cylinder proceeds along its orbit (Figure 2b and c) the free surface oscillates, and a radial flow develops with the left vortical cell pumping fluid toward the right one. Despite the presence of this strong radial swing motion, the

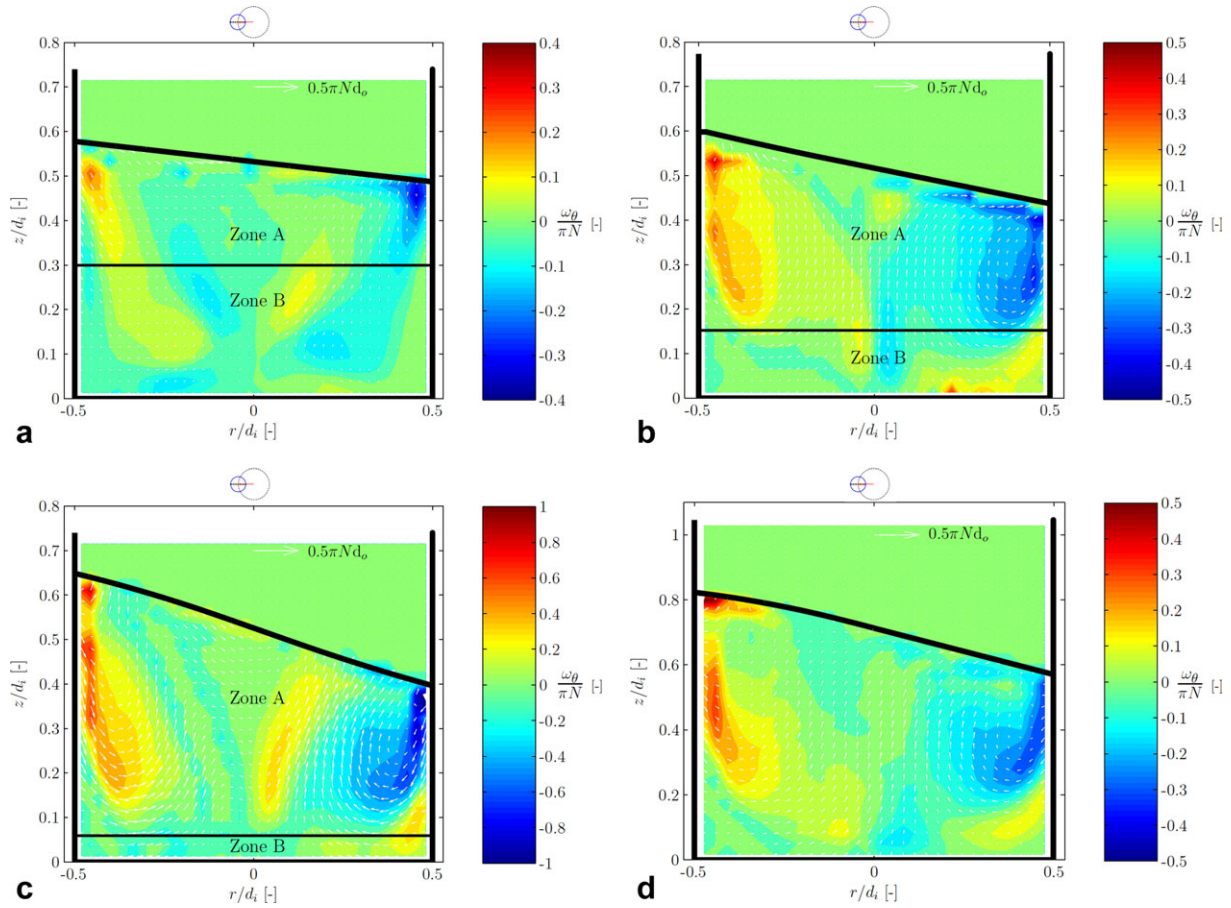

Figure 3. Phase-resolved velocity vector fields and contour plots of the tangential component of the vorticity, ω_θ, for increasing N (d_o/d_i = 0.25, φ = 0°): (a) N = 70 rpm and h/d_i = 0.5, (b) N = 90 rpm and h/d_i = 0.5, (c) N = 110 rpm and h/di = 0.5, and (d) N = 110 rpm and h/d_i = 0.7.

[Color figure can be viewed in the online issue, which is available at wileyonlinelibrary.com.]

two vortical structures are still identifiable from the vorticity contour plots, even if their maximum absolute intensity has decreased and reached a minimum $\|\omega_{\max}/(\pi N)\| = 0.4$, for $\varphi = 90°$ (Figure 2c). With increasing φ the left vortical cell keeps pumping fluid into the right one until the free surface reaches its highest position on the righthand side of the plane of measurement for $\varphi = 180°$.

At this mid-cycle stage a new cycle starts but in this case the radial swing flow is in the opposite direction and the vortical cell on the righthand side pumps fluid into the left one. A more comprehensive understanding of the flow dynamics induced by the free surface oscillation can be gained from the flow reconstruction included in the Supporting Information Video (filename: Shaken.avi), and from the phase lock mixing time measurement video (filename: Mixing.avi).

If the vorticity contours plots of increasing φ are azimuthally stacked after each other a 3-D visualization of the flow can be obtained, denoting the constant presence of an inclined toroidal vortex in the cylinder. The highest/lowest sides of the torus are always aligned with the centrifugal acceleration of the shaker table that changes its direction as φ increases. The ensemble-averaged velocity field and vorticity contour plots are shown in Figure 2d. These plots were purposely made to compare with the simulations carried out by Kim and Kizito,[10] which is the only work available in the literature that provides a qualitative characterization of the flow occurring in an orbitally shaken cylinder. The current results agree well with their emsemble-averaged vector fields for a fluid of analogous viscosity ($\nu = 10^{-6}$ m^2 s^{-1}), with two symmetrical counter-rotating vortices, one on each side of the cylinder. It should be noted that the vorticity range of the ensemble-averaged vector field is approximately half of the vorticity range associated with the phase-resolved flow for $\varphi = 0°$, implying that time-averaged circulation times, controlling macromixing, are approximately double those encountered at the phase angle where the fastest mixing occurs.

Toroidal vortex growth for in-phase condition

The phase-resolved velocity field and vorticity contour plots for three shaking rotational speeds, N = 70, 90 and 110 rpm, are shown in Figure 3a–c) for a nondimensional fluid height $h/d_i = 0.5$ and $\varphi = 0°$, while Figure 4d refers to a fluid height $h/d_i = 0.7$ and N = 110 rpm. Similarly to the flow dynamics described previously for $h/d_i = 0.3$, two counter-rotating vortices can be distinguished in all the plots. As N is increased (Figure 3a–c), the two vortices start to extend toward the bottom of the cylinder and their intensity increases in magnitude, with the maximum absolute nondimensional vorticity being more than double ($\|\omega_{\theta max}/(\pi N)\| = 0.4. \rightarrow 1$).

For N = 110 rpm the two vortices extend over the entire cylinder height (Figure 3c), and completely control the flow inside the bioreactor. The results are consistent with the

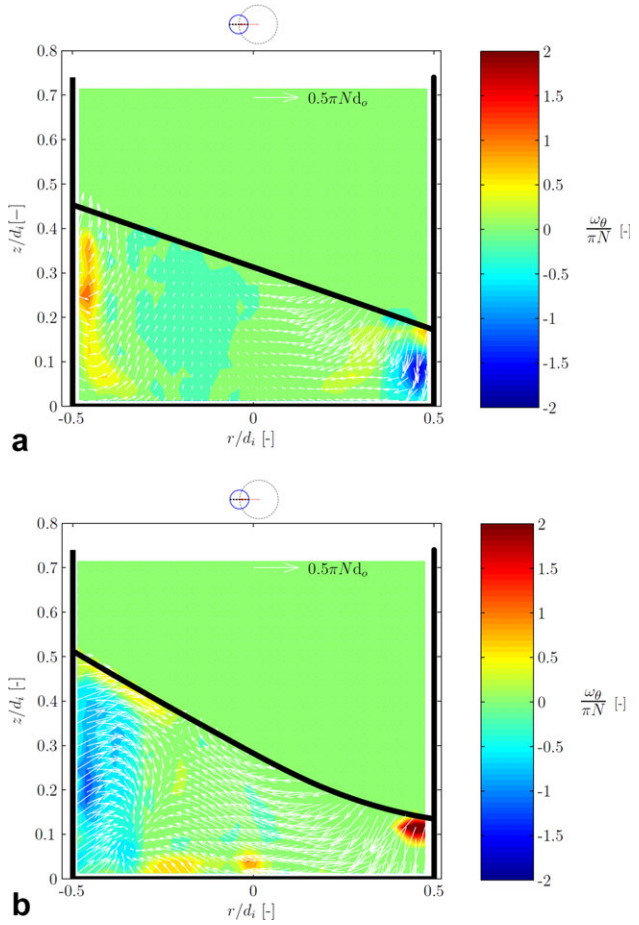

Figure 4. Phase-resolved vector fields and contour plots of the axial component of the vorticity, ω_θ, for increasing N (d_o/d_i = 0.25, φ = 0°): (a) N = 110 rpm and h/d_i = 0.3; (b) N = 130 rpm and h/d_i = 0.3.

[Color figure can be viewed in the online issue, which is available at wileyonlinelibrary.com.]

findings of Tissot et al.[19] who measured the mixing time in a cylindrical shaken bioreactor by means of a colorization technique and reported that for a low-shaking frequency two different zones could be distinguished inside the reactor: a first zone close to the free surface where mixing was enhanced by convection, and a second zone close to the bottom of the cylinder where mixing was dominated by diffusion. Their results corroborate these findings as the two counter-rotating vortices of Figure 3a-d are responsible for the transport processes observed by Tissot et al.[19] in the region below the free surface that they denoted as "convection zone". Similarly the so-called "diffusion zone" can be correlated to those regions of Figure 3a and b below the vortical structure where flow activity is less intense. In Figure 3a-c, the horizontal line provides a visual reference to define the boundary between the convection (Zone A) and the diffusion (Zone B) regions. It should be noted that the line has been drawn by arbitrarily selecting a fixed value of the vorticity ($\|\omega_\theta/(\pi N)\| = 0.1$) and drawing a horizontal line tangent to the lowest part of the vorticity contour value selected.

Figure 3d shows the phase-resolved flow field obtained for $h/d_i = 0.7$ at $\varphi = 0°$ for $N = 110$ rpm. This experiment was performed in order to determine if there was a limit on the expansion of the vortices for a greater fluid height h/d_i. The two zones can be clearly seen, similarly to what was observed for $h/d_i = 0.5$. However, in this case for the highest shaking frequency investigated $N = 130$ rpm (not shown), the flow field exhibited a different behavior as the free surface showed a curved profile and for this liquid height ratio $h/d_i = 0.7$, a shaking frequency N, for which the vortices extend all the way to the bottom of the cylinder was not found.

Characterization of the flow for incipient out-of-phase condition

An "out-of-phase" phenomenon occurs at higher rotational speeds N, and is characterized by an amount of fluid not being in phase with the movement of the table. It has been observed by Büchs et al.[12] that the out-of-phase flow is fully established for $Ph < 1.26$. Such data concern vessels of somewhat different wall/bottom shapes and have been obtained for $Fr > 0.4$, when most of the fluid is spread over the bioreactor walls. The results presented in this section concern lower Fr values, when most of the fluid is in contact with the cylinder base, and, therefore, comparisons with the data of Büchs et al.[12] must be made with care. These measurements indicate that the transition from in-phase to out-of-phase flow takes place gradually and show evidence that the *onset* of out-of-phase flow is already present for $Fr < 0.4$.

The PIV and free surface tracking measurements show that at lower N for in-phase conditions the free surface can be approximated by an inclined elliptical disk, whose longer (shorter) axis is the inclined (horizontal) straight line at the intersection between the free surface for $\varphi = 0°$ ($\varphi = 90°$) and the vertical laser plane. At higher N the free surface becomes 3-D and its intersection with the vertical laser plane exhibits a wavy profile. This analysis is in agreement with the free surface snapshots of Zhang et al.[6] which clearly show the transition of the free surface from an elliptical to a more complex 3-D shape, when the rotational speed is increased. Under these conditions a significant change in the flow pattern occurs. This is well illustrated by the vector field and vorticity contour plots of Figure 4a and b, which were obtained for $N = 110$ rpm and 130 rpm, respectively ($h/d_i = 0.3$, $\varphi = 0°$). When comparing the flow fields produced at 90 rpm (Figure 2a) with that obtained for 110 rpm (Figure 4a), it is evident that as N is increased the two characteristic vortices tend to be pushed toward the walls, and at even greater N, 130 rpm (Figure 4b), the flow pattern changes with the tangential vorticity direction at the two walls being opposite to that of the in-phase flow condition.

The variation in flow pattern is more evident when a comparison is made between the measurements taken on horizontal planes for in-phase (Figure 5a) and incipient out-of-phase (Figure 5b) conditions, for $\varphi = 180°$. Figure 5a and b show the contour plots of the axial vorticity ω_z, and the velocity vector fields at three different planes for different operating conditions with the fluid height and shaking speed being $h/d_i = 0.7$, $N = 70$ rpm and $h/d_i = 0.3$, $N = 130$ rpm, respectively. For $h/d_i = 0.7$ and $N = 70$ rpm ($Fr = 0.068$, in-phase flow), three different horizontal planes are considered: two in the diffusion zone at elevations $z/d_i = 0.1$, and 0.35, and one in the convection zone at an elevation $z/d_i = 0.6$. In the diffusion zone ($z/d_i = 0.1$), the flow is dominated by an axial vortex clearly in evidence near the center of the cylinder, while a more complex flow pattern is present in the convection zone at $z/d_i = 0.6$. A better view of the flow field at this height is provided in the planar view

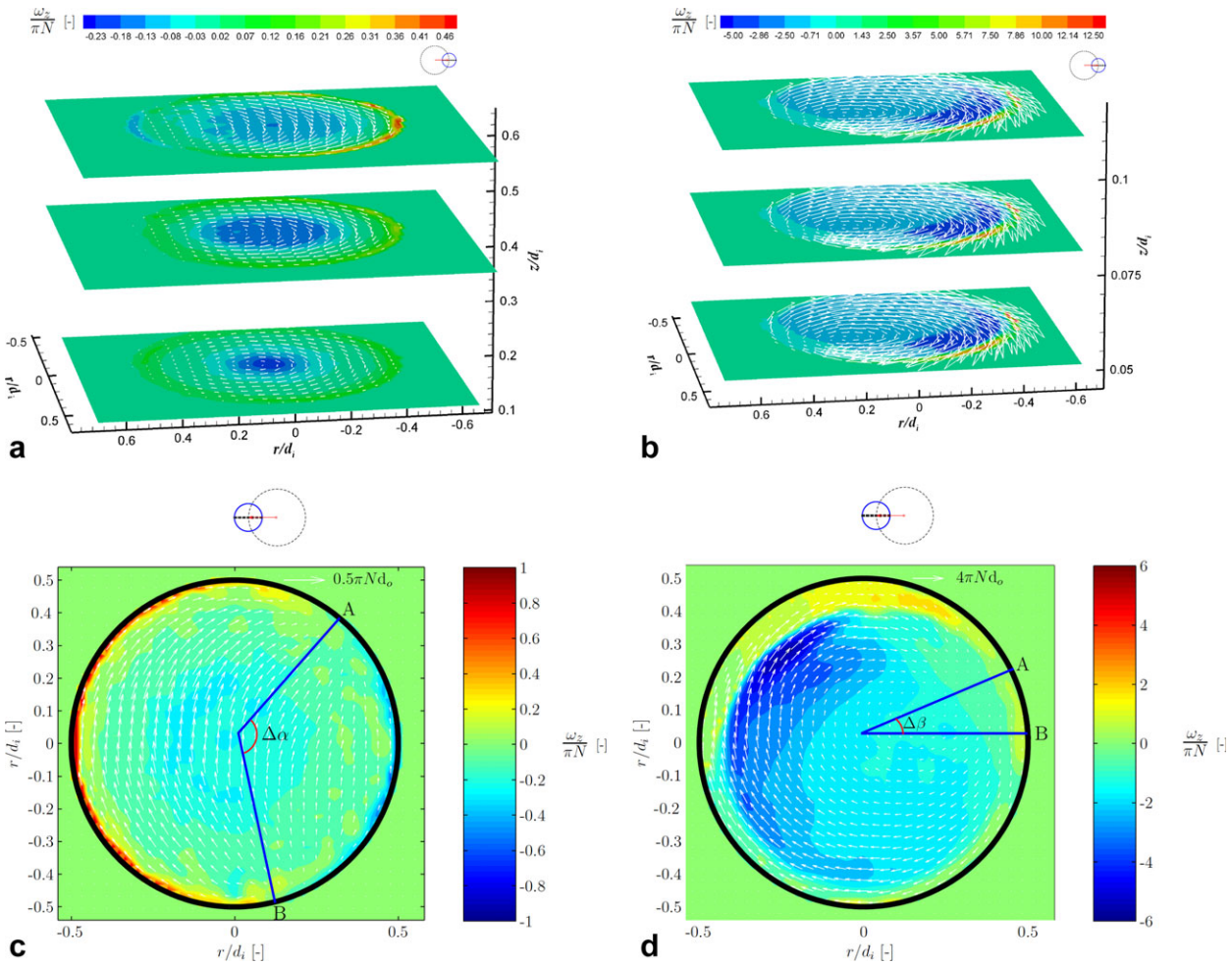

Figure 5. Phase-resolved vector fields and contour plots of the axial component of the vorticity, ω_z, for increasing N (d_o/d_i = 0.25): (a) 3-D view at three z/d_i, N = 70 rpm, h/d_i = 0.7 and φ = 180°, (b) 3-D view at three z/d_i, N = 130 rpm, h/d_i = 0.3 and φ = 180°, (c) top view, z/d_i = 0.075, N = 90 rpm, h/d_i = 0.3 and φ = 0°, and (d) top view, z/d_i = 0.075, N = 130 rpm, h/d_i = 0.3 and φ = 0°.

[Color figure can be viewed in the online issue, which is available at wileyonlinelibrary.com.]

of Figure 5c, where two distinct streams of opposite direction emanating from and merging at the stagnation points denoted as B and A are clearly present.

The variation of the angle, $\Delta\alpha$, between the lines joining the stagnation points to the center of the cylinder, and its relation to the diameter of the toroidal vortex d_v, obtained from the vertical plane measurements is shown in Table 1. For increasing Fr, before flow transition $Fr < 0.11$ (0.17) for $h/d_i = 0.3$ (0.5), it is evident that the angle $\Delta\alpha$ increases together with the toroidal vortex diameter d_v. With the onset of flow transition, both $\Delta\alpha$ and the toroidal vortex diameter decrease as the vortex is pushed toward the wall. When the transition to the out-of-phase condition is induced at a speed of $N = 130$ rpm ($Fr = 0.24$) for $h/d_i = 0.3$ (Figure 5b), the two stagnation points of Figure 5c disappear, and a vortex with a vertical axis is formed on the side of the bioreactor opposite to the highest side of the free surface The intensity of this vertical vortex is similar at each of the elevations considered. This vortex is clearly present in the instantaneous free surface snapshot of Zhang et al.[6] for the greatest speed they considered. It is worth noting that for the incipient out-of-phase condition the maximum intensity of the nondimensional vorticity in the axial direction, ($\|\omega_{max}/(\pi N)\| \approx 5$.), is approximately five times greater than that exhibited for in phase-flow by the tangential vorticity component, ($\|\omega_{\theta max}/(\pi N)\| \approx 1$), for the same height $h/d_i = 0.3$ (cf. Figure 5b and Figure 2a). This implies that nondimensional circulation times for incipient out-of-phase flow are approximately five times smaller than those for in-phase flow. Taking into account all the differences between the two experiments and systems, this value compares reasonably well with the nondimensional mixing time NT, measured by Tissot et al.[19] who for similar rotational speeds of 90 rpm and 110 rpm found dimensionless mixing times of $NT \approx 60$ and ≈ 16, with a ratio of approximately 3.75 between the two.

The extent of the flow transition to out-of-phase can be determined by estimating $\Delta\beta$, the angle defined by the

Table 1. Variation of the Angle $\Delta\alpha$ and of the Ratio of the Toroidal Vortex and Cylinder Diameters d_v/d_i, with Froude Number Fr, for h/d_i = 0.3 and 0.5

	$Fr = 0.069$	$Fr = 0.11$	$Fr = 0.17$	$Fr = 0.24$
$h/d_i = 0.3$	$\Delta\alpha = 105°$	$\Delta\alpha = 128°$	$\Delta\alpha = 71°$	NA
	$d_v/d_i = 0.15$	$d_v/d_i = 0.25$	$d_v/d_i = 0.16$	
$h/d_i = 0.5$	$\Delta\alpha = 103°$	$\Delta\alpha = 135°$	$\Delta\alpha = 148°$	$\Delta\alpha = 88°$
	$d_v/d_i = 0.13$	$d_v/d_i = 0.27$	$d_v/d_i = 0.44$	$d_v/d_i = 0.21$

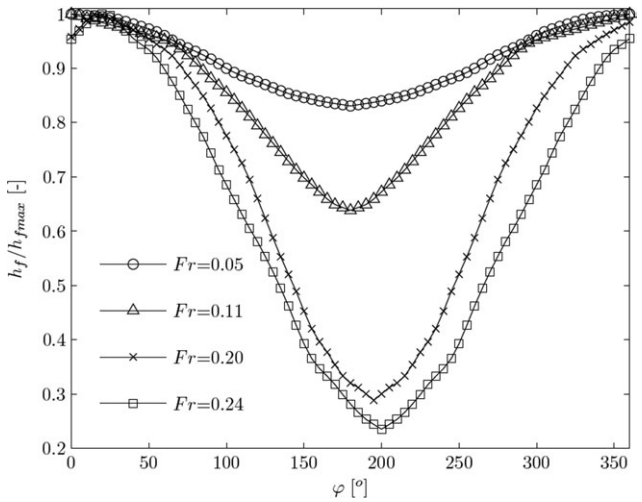

Figure 6. Variation of the nondimensional fluid height at the side of the free surface h_f/h_{fmax}, with phase angle, φ.

direction of the centrifugal acceleration for the phase condition considered (a horizontal line for $\varphi = 0°$), and the direction of the line joining the bioreactor and vortex centers (Figure 5d). For the operating conditions of Figure 5d the out-of-phase angle was found to be $\Delta\beta = 20°$. Experiments were repeated at three different phase angles $\varphi = 0°$, 90° and 180°, and it was found that $\Delta\beta$ is independent of the phase angle considered. It can be concluded that the vertical vortex precesses around the cylinder axis as the tray proceeds along its orbit.

The transition to the out-of-phase flow was further investigated by conducting image analysis of the variation of the height h_f, of the point on the free surface profile at the left wall of the bioreactor for different phase angles φ. Measurements of h_f were carried for the following operating conditions: $h/d_i = 0.3$, $0° < \varphi < 360°$, and $N = 60$ rpm ($Fr = 0.05$), 90 rpm ($Fr = 0.11$), 120 rpm ($Fr = 0.20$), and 130 rpm ($Fr = 0.24$). The variation of $h_f/h_{f\max}$ with φ is shown in Figure 6, where $h_{f\max}$ is the maximum value of h_f. For $Fr = 0.05$ and 0.11, $h_f/h_{f\max}$ is maximum ($h_f/h_{f\max} = 1$) for $\varphi = 0°$, which means that the free surface is in phase with the orbital movement of the shaken bioreactor. At high-shaking speeds $N = 120$ rpm ($Fr = 0.20$) and 130 rpm ($Fr = 0.24$), the maximum value of h_f was found at $\varphi = 15°$ and 20°, respectively. The latter value is in good agreement with the one found at the same speed from the PIV measurements in horizontal planes. These results corroborate the hypothesis that a transition to out-of-phase flow starts being manifested at low values of Fr, and increases with increasing N until the fluid reaches the fully-established out-of-phase conditions reported by Büchs et al.[12]

Flow transition and scaling law

This section aims at deriving a scaling law based on dimensionless parameters that can be used to have more control over the bioprocess by selecting the most appropriate flow conditions. The free surface motion is the flow driving mechanism of the shaken bioreactor, and its maximum inclination θ, is related to the nondimensional wave amplitude $\Delta h/d_i$, according to the expression on the lefthand side of Eq. 5

$$\tan\theta = \frac{\Delta h}{d_i} \propto \frac{a_c}{g} = \left(\frac{2(\pi N)^2 d_0}{g}\right) = Fr \tag{5}$$

From fluid mechanics considerations the local inclination of the free surface is also expected to be proportional to the ratio between the centrifugal acceleration $a_c = (\pi N d_o)^2/(0.5\, d_o)$, determined by the orbital motion and gravity, g (see the expression on the righthand side of Eq. 5). This proportionality is well reflected in Figure 7a, where the variation of $\Delta h/d_i$ is plotted against Fr for different nondimensional fluid heights h/d_i, and nondimensional orbital diameter d_o/d_i. It should be noted that the data of Figure 7a were obtained for two cylinders of diameter $d_i = 10$ cm and 13 cm, and several orbital diameters in the range $d_o = 1.5$–5 cm. From Figure 7a it is evident that at a given Fr, for selected combinations of N and d_o, the free surface will assume a fixed inclination that is independent of the fluid height h/d_i. The linear relationship is more consistent at lower Fr when the flow is in-phase and the free surface inclination is constant across the free surface profile, while at higher Fr, the data are more scattered about the reference line due to the wavy nature of the free surface for transitional out-of-phase conditions. For these conditions the local inclination of the free

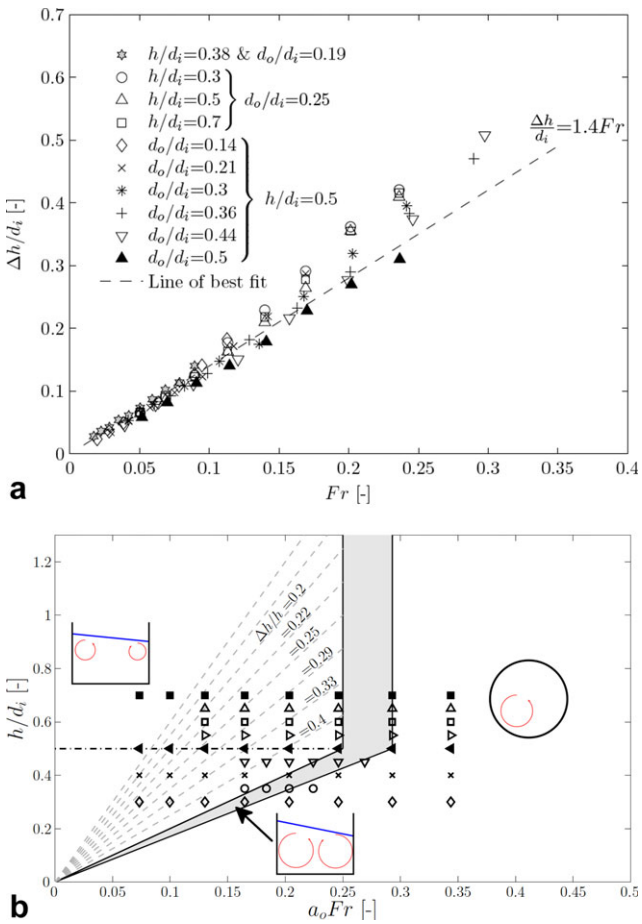

Figure 7. (a) Variation of $\Delta h/d_i$ with Fr; and (b) flow transitional region (gray shaded) from in-phase to onset of out of phase conditions in the h/d_i-Fr plane ($d_0/d_i = 0.25$).

[Color figure can be viewed in the online issue, which is available at wileyonlinelibrary.com.]

surface varies along the radial coordinate, and, therefore, the inclination, $\Delta h/d_i$, reported in Figure 7a is the average across the radial profile. The constant of proportionality, $a_0 = 1.4$, is directly related to the fluid considered (water in this study), and its value is greater than unity because it takes into account the extra inertial forces, besides the centrifugal acceleration of the tray, due to the movement of the fluid inside the cylindrical bioreactor.

For an orbital diameter $d_o/d_i = 0.25$ it was found that the toroidal vortex extends to the bottom of the tank for a nondimensional critical wave amplitude $(\Delta h/h)_c \approx 0.5$. This is also evident from the plots of Figures 2a and 3c for $h/d_i = 0.3$ ($Fr = 0.11$), and 0.5 ($Fr = 0.17$), respectively. In both cases a further increase in Fr would instigate the onset of the out-of-phase condition. Based on these considerations Eq. 5 can be rearranged as in Eq. 6, where the nondimensional fluid height h/d_i is directly and inversely proportional to the Froude number Fr, and the nondimensional wave amplitude, respectively

$$\frac{h}{d_i} = a_0 \frac{h}{\Delta h} Fr \tag{6}$$

Based on Eq. 6 a map of h/d_i, Fr combinations are provided in Figure 7b to help predict the flow transition. Three inset diagrams reproducing the characteristic flows before, at and after flow transition are present at the left, center and righthand sides of Figure 7b, respectively. They are associated with three different regions in the figure, that indicated by the gray shaded area and those on either side of it. It is worth remarking that this map is valid only for $d_o/d_i = 0.25$. Positions on the lefthand side of Figure 7b, at low Fr, are characterized by a toroidal vortex, which is increasing in size as Fr increases (cf. inset diagram on the lefthand side). In this case two regions in the (Fr, h/d_i) plane can be identified before flow transition. For $h/d_i < 0.5$ transition occurs when $h/d_i = 2\ a_0\ Fr$ ($(\Delta h/h)_c \approx 0.5$), while for $h/d_i > 0.5$ it occurs at a constant Fr for $a_o Fr = 0.25$ (cf. Figure 3d for $h/d_i = 0.7$). In the latter case the toroidal vortex does not reach the bottom of the vessel for any Fr. In Figure 7b the gray dashed lines are associated with constant values of $\Delta h/h$, and can be used to determine the extent of the diffusion zone beneath the toroidal vortex. The extent of the diffusion zone decreases as $\Delta h/h$ increases and therefore according to Eq. 6 the slope of lines of greater $\Delta h/h$ decreases and reaches its minimum inclination of 2 at the onset of flow transition for $h/d_i < 0.5$. The data points in the gray shaded area are those where flow transition occurs and the toroidal vortex either reaches the bottom of the tank ($h/d_i < 0.5$), or grows to its maximum size ($h/d_i > 0.5$). To the right of the gray shaded area, at greater Fr, the flow is characterized by a vertical axial vortex as shown by the inset flow diagram on the righthand side of Figure 7b. The data points in Figure 7b represent the combinations of h/d_i and Fr that have been tested with both the PIV and the free surface image analysis to validate the proposed methodology to identify flow transition.

To extend the methodology developed for $d_o/d_i = 0.25$, further PIV measurements were carried out for different d_o/d_i. Figures 8a and b show the characteristic vector fields of incipient flow transition (toroidal vortex reaching to the bottom of the tank) for two different combinations of tank sizes and orbital diameters, $d_o/d_i = 0.4$ ($d_o = 4$ cm and $d_i =$ 10 cm) and $d_o/d_i = 0.115$ ($d_o = 1.5$ cm and $d_i = 13$ cm) and the same nondimensional height $h/d_i = 0.3$. From the free surface inclination the critical wave amplitudes are $(\Delta h/h)_c \approx 0.66$ and $(\Delta h/h)_c \approx 0.34$ in Figure 8a and b, respectively.

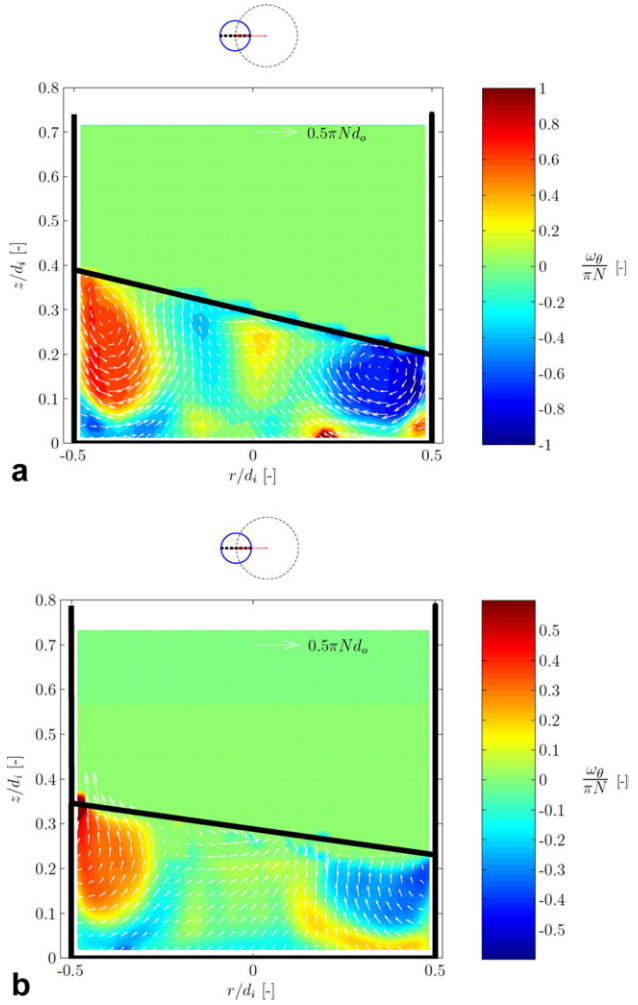

Figure 8. Phase-resolved vector fields and contour plots of the tangential component of the vorticity, ω_θ, for: (a) N = 77 rpm, φ = 0°, d_o/d_i = 0.4 and h/d_i = 0.3 (d_i = 10 cm), and (b) N = 95 rpm, φ = 0° d_o/d_i = 0.115 and h/d_i = 0.3 (d_i = 13 cm).

[Color figure can be viewed in the online issue, which is available at wileyonlinelibrary.com.]

The variation of the critical wave amplitude $(\Delta h/h)_c$ with d_o/d_i for two different fluid heights $h/d_i = 0.3$ and 0.5, and two different tank sizes $d_i = 10$ cm (white symbols), and 13 cm (gray symbols) is shown in Figure 9. The current results show that the critical wave amplitude, $(\Delta h/h)_c$, increases with increasing d_o/d_i, and can be modeled with a square root power law. This behavior is also visible in the data reported in Figure 7a. Data associated with higher values of d_o/d_i deviate from the linear relationship related to the toroidal vortex flow at a greater Fr, and, therefore, at a greater inclination θ (see Eq. 5). For example data-points of $d_o/d_i = 0.5$ are still close to the linear relationship at $Fr = 0.25$, while for $d_o/d_i = 0.25$ they deviate at $Fr = 0.15$ (see Figure 7a). The reason for this behavior can be explained by considering two hypothetical flow configurations for a given inner

diameter d_i and fluid height h with $d_{o1} < d_{o2}$. When the critical Froude number Fr_{c1} is achieved, both configurations will exhibit the same wave amplitude Δh (or free surface inclination θ), but the rotational speed of configuration 1 will be greater than that of configuration 2, and, therefore, the free surface vertical speed, $(\Delta hN)_1$, will be also greater than that of configuration 2, $(\Delta hN)_2$. In other words, configuration 2 associated with the greater d_o will not experience the flow transition at Fr_{c1} because its free surface vertical speed is not large enough to push the circulation of the toroidal vortex to the bottom of the tank. This is well summarized in Eq. 7, derived from $(\Delta h/h)_c = (d_o/d_i)^{0.5}$, which shows the ratio of critical wave speeds for two configurations with same nondimensional fluid height, h/d_i, as a function of the Fr_c and d_i ratios. In particular for a constant d_i, the ratio of the critical wave speeds must be equal to the square root of the critical Froude number ratio, and, therefore, of the critical centrifugal accelerations

$$\frac{(\Delta h_c N_c)_1}{(\Delta h_c N_c)_2} = \sqrt{\frac{(d_0/d_i)_1}{(d_0/d_i)}}\frac{N_{c1}h_1}{N_{c2}h_2} = \sqrt{\frac{Fr_{c1}}{Fr_{c2}}}\sqrt{\frac{d_{i1}}{d_{i2}}} \tag{7}$$

The flow transition map of Figure 7b is valid only for $d_o/d_i = 0.25$, and can be extended to different orbital to cylinder diameter ratios d_o/d_i, by redrawing the inclined and vertical transition lines after substitution of the critical wave amplitude $(\Delta h/h)_c = (d_o/d_i)^{0.5}$ in Eq. 6. When the nondimensional fluid height $h/d_i > (d_o/d_i)^{0.5}$, flow transition will occur without the vortex reaching the bottom of the tank and a diffusion zone will be present. This latter condition is occurring in the map of Figure 7b for $h/d_i > 0.5$ when $d_o/d_i = 0.25$. In this case the transitional velocity for a given configuration does not depend on the orbital diameter but is limited by the inner cylinder diameter and can be found from Eq. 8

$$a_0 Fr_{d_i} = 1 \tag{8}$$

where Fr_{di} is the Froude number based on the cylinder dia. d_i.

To conclude, when the nondimensional fluid height $h/d_i < (d_o/d_i)^{0.5}$ the transitional speed can be derived from Eq. 6 by using the critical wave amplitude $(\Delta h/h)_c=(d_o/d_i)^{0.5}$, while

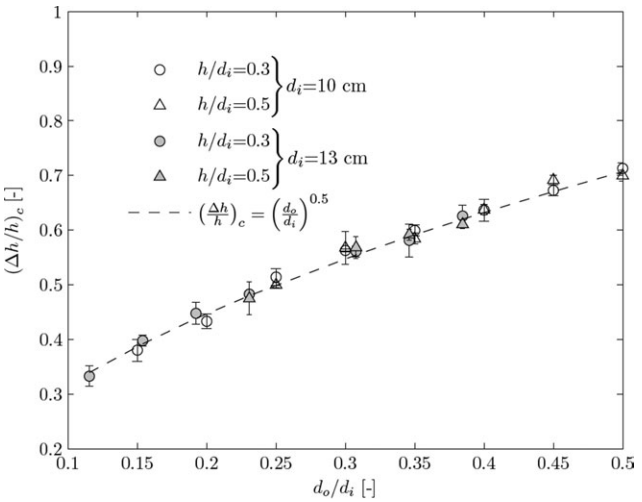

Figure 9. Variation of the nondimensional critical wave amplitude $(\Delta h/h)_c$, with increasing orbital to cylinder diameter ratio d_o/d_i.

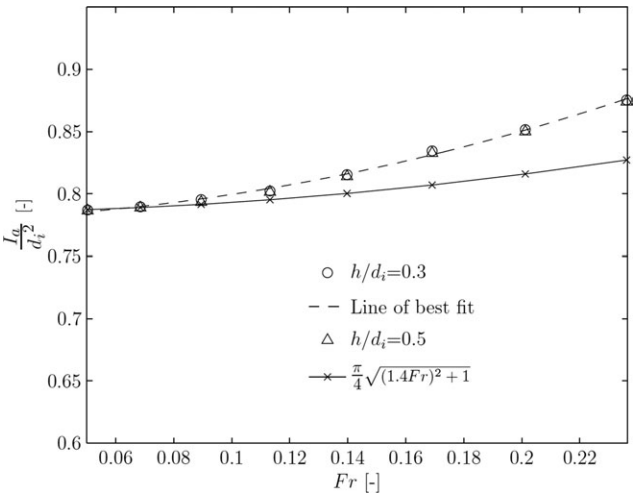

Figure 10. Variation of the nondimensional interfacial area I_a, with increasing Fr for d_o/d_i = 0.25.

for $h/d_i > (d_o/d_i)^{0.5}$ Eq. 8 must be used. The proposed scaling law was also assessed against the experimental free surface visualization of Zhang et al.[6] which shows flow transitions occurring at rotational speeds in the range 80–100 rpm and 60–80 rpm for a 5 L and 30 L bioreactor, respectively. Their data show a good agreement with these results, and the model proposed in this work predicts transitional speeds of 86 rpm and 66 rpm. These values were estimated from Eq. 8, because $h/d_i > (d_o/d_i)^{0.5}$ in both configurations.

Interfacial area

Direct estimates of the free surface interfacial area I_a were obtained by azimuthally stacking the different free surface profiles measured at each phase angle φ, and by integrating the reconstructed 3-D free surface. An analytical solution of I_a was also derived in Eq. 9. This is based on the assumption that the free surface is an inclined elliptical disk and is valid at low Fr, when the free surface profile at $\varphi = 0^\circ$ is an inclined line

$$\frac{I_a}{d_i^2} = \frac{\pi}{4}\sqrt{(1.4Fr)^2 + 1} \tag{9}$$

A comparison between the analytical and measured interfacial areas obtained for an orbital diameter $d_o/d_i = 0.25$ is made in Figure 10. The two estimates of the interfacial area show a relatively good agreement for $Fr < 0.15$. Before flow transition the maximum discrepancy between the two estimates is 2%, well within the error in the detection of the free surface profile. At higher Fr the measured interfacial area deviates from the analytical solution because flow transition takes place and the free surface exhibits a wavy profile. It is worth noting that these data indicate that the interfacial area is independent of the fluid liquid height for the two h/d_i tested. This can be explained by considering that the free surface maximum inclination is independent of the amount of fluid present in the vessel and is determined only by the centrifugal acceleration experienced by the fluid and therefore by Fr.

Conclusions

This study has provided a detailed and improved understanding of the flow dynamics inside a shaken bioreactor. The measurements revealed that the flow consisted mostly of

two counter-rotating vortices, observed near the free surface for $\Delta h/h < (d_o/d_i)^{0.5}$, that strongly affect the mixing process. These vortices extended all the way to the bottom of the cylinder when the critical wave amplitude $(\Delta h/h)_c = (d_o/d_i)^{0.5}$ is reached.

With increasing rotational speed, the two counter-rotating vortices first move toward the vessel wall and then subsequently disappear, when an incipient flow transition to out-of-phase flow is in evidence. Measurements in horizontal planes were also made in order to elucidate further the flow behavior. A vertical vortex precessing around the cylinder was identified for high Fr flow; the center of this vertical vortex was out-of-phase with respect to the axis of the shaker table. Free surface image analysis showed that the extent of out-of-phase flow increased with Fr. The results confirmed the presence of out-of-phase flow at high rotational speeds or Fr, in agreement with the findings of Büchs et al.[12] Furthermore, the detailed flow field data obtained show clear evidence that incipient transition to out-of-phase flow starts at Froude number lower than the $Fr > 0.4$ considered by Büchs et al.[12]. The scaling laws of Eqs. 6 and Eqs. 8 for $h/d_i < (d_o/d_i)^{0.5}$ and $h/d_i > (d_o/d_i)^{0.5}$ are proposed to improve bioprocess design by predicting the flow transition occurring in the bioreactor and by scaling similar flow conditions in cylindrical bioreactors of different sizes.

The free surface interfacial area was directly measured for $0.05 < Fr < 0.24$, and it was found to compare well with a derived analytical solution at low Fr when the flow is fully in-phase with the orbital motion of the cylinder and the free surface can be approximated by an elliptical disk.

The results presented in this article throw light on the detailed flow characteristics of shaken bioreactors and on the influence of critical nondimensional operating parameters on the transport phenomena of such vessels. Such characteristics can help guide the selection of feed insertion locations to improve the mixing performance; physical insight suggests that insertion at the edges of the vortical structures should produce faster mixing, but this is at present being investigated through mixing time measurements. Further work on the variation of circulation times, shear rates and local viscous dissipation rates with flow parameters and the influence of different fluid viscosities on the mixing dynamics of the bioreactor is also called for. Experiments to elucidate such effects are in progress and shall be reported in a later publication.

Acknowledgments

Financial support from the Engineering and Physical Sciences Research Council of the U.K (grant ref. EP/E055958) for the work reported here is acknowledged. The authors also thank Kühner AG for their support.

Notation

Abbreviations

2-D = two-dimensional
3-D = three-dimensional
CFD = computational fluid dynamics
PIV = particle image velocimetry

Greek letters

$\Delta\alpha$ = angle between two stagnation points
$\Delta\beta$ = angle delay of the precessional vortex
φ = phase angle of the table
θ = angle of the free surface
ω_i = vorticity component in the ith direction, s^{-1}
v = fluid viscosity, $m^2 s^{-1}$

Roman symbols

a_o = = *constant*
d_i = inner diameter of the cylinder, m
d_o = orbital diameter, m
d_v = toroidal vortex diameter, m
F_c = centrifugal force, Kg m s^{-2}
F_g = gravitational force, Kg m s^{-2}
g = gravitational acceleration, m s^{-2}
h = fluid height, m
h_f = fluid height at the lefthand side wall, m
Δh = free surface height, m^2
I_a = free surface interfacial area, m^2
N = shaker table rotational speed, s^{-1}
Ph = phase number
P_v = volumetric power consumption, Kg m^{-1} s^{-2}
V_f = fluid volume, m^3
u_i = velocity component in the ith direction, ms m^{-1}

Literature Cited

1. Büchs J. Introduction to advantages and problems of shaken cultures. *Biochem Eng J*. 2001;7:91–98.
2. Escudie R, Bouyer D, Line A. Characterization of trailing vortices generated by a Rushton turbine. *AIChE J*. 2004;49(3): 585–603.
3. Lavery M, Nienow AW. Oxygen transfer in animal cell culture medium. *Biotech Bioeng*. 1986;30(3):368–373
4. Lara AR, Galindo E, Ramírez OT, Palomares LA. Living with heterogeneities in bioreactors. *Molec Biotechnol*. 2006;34:355–381.
5. Klöckner W, Büchs J. Advances in shaking technologies. *Trends Biotechnol*. 2012;30:307–314.
6. Zhang X, Bürki C, Stettler M, De Sanctis D, Perrone M, Parolini N, Discacciati M, De Jesus M, Hacker D, Quarteroni A, Wurm F. Efficient oxygen transfer by surface aeration in shaken cylindrical containers for mammalian cell cultivation at volumetric scales up to 1000 L. *Biochem Eng J*. 2009;45:41–47
7. Zhang X, Stettler M, De Sanctis D, Perrone M, Parolini N, Discacciati M, De Jesus M, Hacker D, Quarteroni A, Wurm F. Use of orbital shaken disposable bioreactors for mammalian cell cultures from the milliliter-scale to the 1,000-liter scale. *Adv Biochem. Eng Biotechnol*. 2010;115:33–53.
8. Zhang H, Williams-Dalson W, Keshavarz-Moore E, Ayazi-Shamlou P. Computational fluid dynamics (CFD) analysis of mixing and gas liquid mass transfer in shaken flasks. *Biotech Appl Biochem.* 2005;41:1–8.
9. Zhang H, Lamping S, Pickering S, Lye G, Ayazi-Shamlou P. Engineering characterization of a single well from 24-well and 96-well microtiter plates. *Biochem Eng J*. 2008;40:138–149.
10. Kim H and Kizito P. Stirring free surface flows due to horizontal circulatory oscillation of partially filled container. *Chem Eng Commun*. 2009;11:1300–1321.
11. Discacciati M, Hacker D, Quarteroni A, Quinodoz S, Tissot S, Wurm F. Numerical simulation of orbitally shaken viscous fluids with free surface. *Int J Numer Meth Fluids*. 2012. doi:10.1002/fld.3658.
12. Büchs J, Maier U, Milbradt C, Zoels B. 2000. Power consumption in shaking flasks on rotary shaking machines: II. Nondimensional description of specific power consumption and flow regimes in unbaffled flasks at elevated liquid viscosity. *Biotechnol Bioeng*. 2000;68:594–601.
13. Bouremel Y, Yianneskis M, Ducci A. On the utilisation of vorticity and strain dynamics for improved analysis of mixing in stirred vessels. *Chem Eng Res Des*. 2009;87:377–385.
14. Doulgerakis Z, Yianneskis M, Ducci A. On the manifestation and nature of macroinstabilities in stirred vessels. *AIChE J*. 2011;57: 2941–2954.
15. Ducci A, Yianneskis M. Direct determination of dissipation rate in a stirred vessel with multi-channel LDA. *AIChE J*. 2005;51:2133–2149.
16. Ducci A, Yianneskis M. Turbulence kinetic energy transport processes in the impeller stream of stirred vessels. *Chem Eng Sci*. 2006;61: 2780–2790.

17. Ducci A, Doulgerakis Z, Yianneskis M. Decomposition of flow structures in stirred reactors and implications for mixing enhancement. *Ind Eng Chem Res*. 2008;47:3664–3676.
18. Weheliye W, Yianneskis M, Ducci A. 2012. PIV measurements in a shaken cylindrical bioreactor. In: Proceedings of the 16th Int. Symposium on Applications of Laser Techniques to Fluid Mechanics; 9–12 July, Lisbon, Portugal. Paper 4.1.1. http://ltces.dem.ist.utl. pt/lxlaser/lxlaser 2012 /program.asp.
19. Tissot S, Farhat M, Hacker D, Anderlei T, Kühner M. Determination of a scale up factor from mixing time studies in orbitally shaken bioreactors. *Biochem Eng J*. 2010;52:181–186.
20. Massey BS. *Mechanics of Fluids*. London, UK: Chapman and Hall; 1990.

Manuscript received Aug. 9, 2012, and revision received Oct. 3, 2012.